Journal of Materials Chemistry C

PAPER

View Article Online
View Journal | View Issue

Cite this: J. Mater. Chem. C, 2018, 6, 588

Aluminium/gallium, indium/gallium, and aluminium/indium co-doped ZnO thin films deposited *via* aerosol assisted CVD

Dominic B. Potter, Michael J. Powell, Ivan P. Parkin and Claire J. Carmalt *

Received 1st September 2017,
Accepted 7th November 2017

DOI: 10.1039/c7tc04003b

rsc.li/materials-c

Aluminium/gallium co-doped ZnO (AGZO), indium/gallium co-doped ZnO (IGZO), and aluminium/indium co-doped ZnO (AIZO) thin films were synthesised on glass substrates *via* aerosol assisted chemical vapour deposition (AACVD). The films were fully characterised by X-ray diffraction, X-ray photoelectron spectroscopy and scanning electron microscopy. The optoelectronic properties of the films were determined using UV/vis spectroscopy and Hall effect measurements. The AGZO film displayed the lowest resistivity (1.3×10^{-2} Ω cm) and highest carrier mobility (7.9 $cm^2 V^{-1} s^{-1}$), due the relatively low amount of disorder in the structure. The incorporation of In^{3+} resulted in the most disorder in the structure due to its large radius, which led to an increase in optical absorption, and a decrease in resistivity.

Introduction

Doped zinc oxide is a widely investigated material, due to its potential as a sustainable transparent conducting oxide (TCO). TCOs are materials which are both optically transparent and electrically conductive – two properties which are usually mutually exclusive.[1] This combination of functional properties means that TCOs have a broad range of applications in photovoltaic devices, such as solar cells, touch screens, light-emitting diodes (LEDs) and liquid crystal displays (LCDs).[2,3] Commercially, the two most commonly used TCO materials are tin-doped indium oxide (ITO) and fluorine-doped tin oxide (FTO). However, the price of both indium and tin are relatively high and unstable compared to zinc.[4] For this reason, there has been extensive research done into ZnO, due to its inherent *n*-type conductivity,[5–7] as well as its wide, direct band gap (*ca.* 3.37 eV at room temperature),[8–10] low cost,[11–13] and relatively low toxicity,[14–16] all of which make it appealing for industrial processes.

Many dopants have been screened to improve the electrical properties of ZnO. The most common of these are the group 13 elements: aluminium, gallium and indium. These dopants are introduced as substitutional defects on zinc sites.[17] Aluminium-doped ZnO (AZO), gallium-doped ZnO (GZO), and indium-doped ZnO (IZO) thin films have been prepared by various techniques, including magnetron sputtering,[18–20] pulsed laser deposition (PLD),[21–23] molecular beam epitaxy (MBE),[24,25] atomic layer deposition (ALD),[26–28] spray pyrolysis,[29,30] atmospheric pressure chemical vapour deposition (APCVD),[31–33] and aerosol assisted chemical vapour deposition (AACVD).[34–36]

Moreover, co-doped ZnO films have been prepared using these dopants. Co-doping allows the benefits of two dopants to be exploited simultaneously. The strengths of one dopant can compensate for the weaknesses of another. For example, aluminium is the third most abundant element in the Earth's crust.[37] Hence, it is can be purchased at a lower cost than gallium and indium. Furthermore, aluminium has a relatively low toxicity compared to the other elements of group 13.[38] Additionally, AZO films tend to be more conductive than GZO and IZO films.[39–41] However, the high reactivity of aluminium may lead to unwanted side reactions during film growth.[42]

Conversely, gallium is a relatively stable dopant element, which means the potential for unwanted side reactions is lower compared to other dopants.[43–45] Nomoto *et al.* found that, when exposed to 85% humidity at 85 °C for 1000 hours, the resistivity of GZO films were more stable in comparison to AZO films.[46] Another benefit of using gallium as the dopant for ZnO is that the radius of 4-coordinate Ga^{3+} (0.62 Å) is closer to that of 4-coordinate Zn^{2+} (0.74 Å), in comparison to Al^{3+} (0.53 Å) and In^{3+} (0.81 Å).[47] For this reason, it typically results in fewer lattice distortion and crystal defects when it substitutes for Zn^{2+}.[48]

Aluminium/gallium co-doped ZnO (AGZO),[49–51] indium/gallium co-doped ZnO (IGZO),[52–55] and aluminium/indium co-doped ZnO (AIZO)[56–58] thin films have been prepared previously by various techniques. However, until this study, they had not been synthesised *via* AACVD. AACVD is a technique which has several advantages over traditional APCVD. AACVD relies on dissolving the precursors and then generating an aerosol mist from the solution. Hence, the main benefit of AACVD is that a wide range

Materials Chemistry Centre, Department of Chemistry, University College London, 20 Gordon Street, London, WC1H 0AJ, UK. E-mail: c.j.carmalt@ucl.ac.uk

of non-volatile precursors can be used to deposit a film at a low cost. Additionally, it is relatively easy to control the stoichiometry of dopants, since the amount of dopant incorporated into the film is related to the amount used in solution. In general, a higher dopant concentration in solution leads to a higher dopant concentration in the resultant film. Finally, neither the precursors, nor the lines leading to the reactor need to be heated, and hence AACVD is a relatively low-cost technique, through which films can be deposited with ease.[59,60] In addition, recent work by Powell *et al.* has demonstrated that AACVD can be used to deposit films with high growth rates (*ca.* 100 nm min^{-1}), making the technique suitable for certain industrial depositions.[61]

In this paper, AGZO, IGZO, and AIZO thin films were deposited *via* AACVD for the first time. This was also the first time where all three of these materials were synthesised under the same conditions, which has allowed for an unprecedented and thorough comparison of the three co-doped materials. The effects of aluminium, gallium, and indium were investigated with respect to the crystal and grain growth of the films, and the resultant optoelectronic properties. The effects of the dopants can be related to lattice distortion, based on the different ionic radii.

Experimental

Film synthesis

Aerosol assisted chemical vapour deposition (AACVD) was set up as described previously.[36,62] All chemicals were purchased from Sigma-Aldrich, and were used as-bought, without any further purification. A typical precursor solution was made by dissolving $Zn(acac)_2$ (0.50 g, 1.90 mmol) in methanol (20 mL). Following this, dopant quantities of MCl_3 (M = Al, Ga, In) were dissolved in the solution. It was observed previously that 10 mol% dopant led to superior optoelectronic properties of AZO, GZO, and IZO thin films deposited *via* AACVD.[36] For this reason, the total dopant concentration for the co-doped films was kept at 10 mol%. Acetic acid (1 mL) was added to prevent hydrolysis of the $Zn(acac)_2$. The solution was stirred for at least 10 minutes in a glass bubbler. The substrate used was a 3.2 mm thick float glass plate (Pilkington Technology Management Limited, Lancashire, UK), precoated with a 50 nm thick SiO_2 barrier layer to prevent leeching of ions between the substrate and the film. The substrate was cut to an area of 15 cm × 4 cm. It was then cleaned using soapy water, isopropyl alcohol, and acetone, before being loaded horizontally into the reactor, on top of a carbon heating block, which heated the substrate to 450 °C. A top plate was suspended above the substrate to maintain laminar flow of the aerosol. An aerosol mist of the precursor solution was generated using a 'Liquifog' piezo ultrasonic atomizer from Johnson Matthey, which uses an operating frequency of 1.6 MHz. Nitrogen gas (99.99%, BOC) was used to transport the aerosol to the substrate, at a flow rate of 1 L min^{-1}. The exhaust of the reactor was vented into a fume hood. When the precursor solution and the associated aerosol mist had been completely emptied from the bubbler (*ca.* 30 min), the substrate was left to cool naturally under a continuous flow of nitrogen gas. Once cool, the films were handled and stored in air.

Characterisation techniques

X-ray diffraction (XRD) patterns were recorded using a Bruker D8 Discover X-ray diffractometer using monochromatic Cu $K\alpha_1$ and $K\alpha_2$ radiation of wavelengths 1.54056 and 1.54439 Å respectively, emitted in an intensity ratio of 2 : 1, with a voltage of 40 kV and a current of 40 mA. The incident beam angle was in a grazing setup at 1°, and data was collected between 10° and 66° 2θ with a step size of 0.05° at 2 s per step. X-ray photoelectron spectroscopy (XPS) was performed using a Thermo Scientific K-alpha spectrometer with monochromated Kα radiation, a dual beam charge compensation system and constant pass energy of 50 eV, with a spot size of 400 μm. High resolution scans were performed of the carbon 1s, zinc 2p, oxygen 2p, aluminium 2p, gallium 3d, and indium 3d regions. Scans were performed at the film surfaces, and in the bulks of the films after etching for 200 s. Data was fitted using CasaXPS software. Scanning electron microscope (SEM) images were obtained using a JEOL JSM-6301F SEM at an acceleration voltage of 5 kV. UV/vis spectroscopy was done using a Perkin Elmer Lambda 950 UV/vis/NIR Spectrophotometer in both transmission and in diffuse reflectance mode. Room temperature Hall effect measurements were carried out on an Ecopia HMS-3000, which utilises the van der Pauw method. Measurements were taken using a 0.58 T permanent magnet and a current of 1 mA.

Results and discussion

Film synthesis

Aluminium/gallium co-doped ZnO, indium/gallium co-doped ZnO, and aluminium/indium co-doped ZnO thin films were successfully deposited on glass substrates *via* AACVD. Each dopant was kept at 5 mol% relative to zinc in solution, thus giving a total dopant level of 10 mol% in each precursor solution. This was done because previous work has shown that a 10 mol% dopant level for AZO, GZO, and IZO films deposited in the same conditions resulted in superior electrical conductivites.[36] Each deposition was repeated at least three times. No difference was observable between depositions, indicating the reproducibility of the technique.

The films were highly adhesive to the glass substrates. They passed the Scotch tape test, and could not be marked when scratched lightly with a steel scalpel. The films were visibly transparent, and had coloured interference fringes across the surface. These fringes are the result of constructive and destructive interference between photons that reflect from the air-film boundary and the photons that reflect from the film-substrate boundary.[63] The presence of interference fringes indicates that difference in thickness of some regions of the film were similar to the wavelength of visible light.[64]

Crystal structure

All of the as-deposited films consisted of pure wurtzite ZnO. No secondary phases corresponding to Al_2O_3, Ga_2O_3, In_2O_3, or any ternary Zn–M–O (M = Al, Ga, In) compound were detected in the XRD patterns (Fig. 1).

In a thin film, preferred orientation is often observed in the XRD pattern. This is because the grains cannot be completely randomly oriented as is the case for a powder. For a film, growth is restricted in certain directions, which leads to strain.[62] In ZnO, the (002) plane has the lowest surface energy, and hence undoped ZnO films typically show preferred growth in this direction.[65,66] The AGZO film also displayed preferred orientation in the (002) plane. This is analogous to AZO and GZO films deposited using the same conditions.[36] Conversely, the IGZO film did not display preferred orientation in the (002) plane. Rather, the most intense peaks in its XRD pattern were those corresponding to the (100) and (101) planes. This was analogous to the individually doped IZO films deposited in the same conditions.[36] The preferred orientation of the AIZO film appeared to be an amalgamation of the AGZO and IGZO films, with preferred growth in both the (002) and the (101) directions. From these results, it seems evident that the incorporation of aluminium into ZnO promoted growth in the (002) direction, whereas indium promoted growth in the (101) direction. Gallium seems to have had less of an effect over preferred orientation.

In addition, the Scherrer equation was used to estimate the crystallite sizes, from the full-width at half maximum (FWHM) values of the (002) peak for each film:

$$D = \frac{k\lambda}{\beta \cos\theta}$$

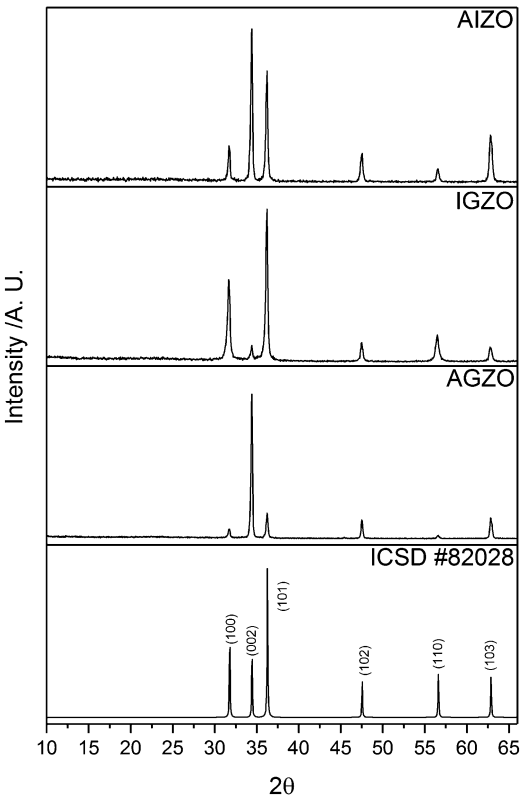

Fig. 1 XRD patterns of AGZO, IGZO, and AIZO films deposited *via* AACVD, using $Zn(acac)_2$ and MCl_3 in methanol, at a deposition temperature of 450 °C. A diffraction pattern of ZnO from ICSD #82028 is included for reference.

where D is the crystallite size, k is the Scherrer constant (taken to be 0.9), λ is the wavelength of the incident X-rays, β is the FWHM in radians, and θ is the Bragg diffraction angle in radians.[67] It was found that the crystallite sizes of AGZO, IGZO, and AIZO were 80 nm, 76 nm and 60 nm, respectively. Hence, the sharp peaks of the AGZO film indicated high quality crystal growth, with relatively large crystallites.[68] This is ideal for TCO applications, as it will lead to a reduction of scattering at crystal defects, consequently resulting in improved carrier properties.[69] A reduction in crystallite size for the films synthesised with indium indicates that indium was hindering crystallite growth. Nguyen *et al.* noted that the presence of indium resulted in a deterioration in crystal quality for their IGZO film deposited *via* magnetron sputtering, compared to their GZO film.[55] Similarly, Teehan *et al.* reported a deterioration in crystal quality of their AIZO films deposited *via* magnetron sputtering, compared to their AZO film.[56] Both groups attributed the resultant peak broadening to the larger ionic radius of In^{3+}, which led to relatively poor quality crystal growth. The AIZO film had the smallest crystallites compared to AGZO and IGZO. This may be due to the lack of gallium, which is the dopant whose ionic radius is the most similar to that of Zn^{2+}. Since the ionic radii of aluminium and indium are further from that of Zn^{2+}, they will increase local strain, and prevent high quality crystal growth.

Elemental analysis

The oxidation states of the elements in the films were determined by XPS. Adventitious carbon was used to calibrate the data, with a binding energy of 285.0 eV for the carbon 1s peaks.[70,71] The binding energies of the zinc $2p_{3/2}$ and $2p_{1/2}$ peaks were consistently found to be 1021.3 eV (±0.2 eV) and 1044.4 eV (±0.2 eV), respectively, which can be attributed to the Zn^{2+} in ZnO (Fig. 2a and b).[72,73] The oxygen 2p peaks for the films could be deconvoluted into three separate peaks, O_I, O_{II}, and O_{III}, with binding energies of 530.0 eV (±0.2 eV), 531.6 eV (±0.2 eV), and 532.6 eV (±0.2 eV), respectively (Fig. 2c and d). O_I, the most intense peak, can be attributed to the O^{2-} ions in ZnO.[16] O_{II} can be attributed to O^{2-} ions located in oxygen deficient regions in ZnO, and thus relates to the concentration of oxygen vacancies (V_O).[16,43,55,74,75] O_{III} can be attributed to surface bound oxygen species, such as O_2^-, $-CO_3$, and H_2O.[73,76] Upon etching, the oxygen environments changed, with the relative intensities of the O_{II} and O_{III} peaks diminishing significantly. This indicates that the surface bound impurities were mostly (but not completely) removed by the etching process. It also suggests that the V_O concentration decreased within the bulks of the films. Wong *et al.* observed that there was a higher concentration of oxygen vacancies at the surfaces of their ZnO nanowires, deposited *via* CVD.[77] They explained this by calculating that V_O formation energy is lower near the surface than it is in the bulk. This was confirmed by Deng *et al.*, who also found that V_O migration in ZnO is energetically favourable in the direction from the bulk to the surface.[78] Carrasco *et al.* also stated that there is a low diffusion barrier for V_O in ZnO.[79] These results all agree with our experimental observations.

All of the dopants were successfully incorporated into the ZnO lattices (Fig. 3). The aluminium $2p_{3/2}$ and $2p_{1/2}$ peaks had binding energies of 75.1 eV (±0.2 eV) and 75.5 eV (±0.2 eV),

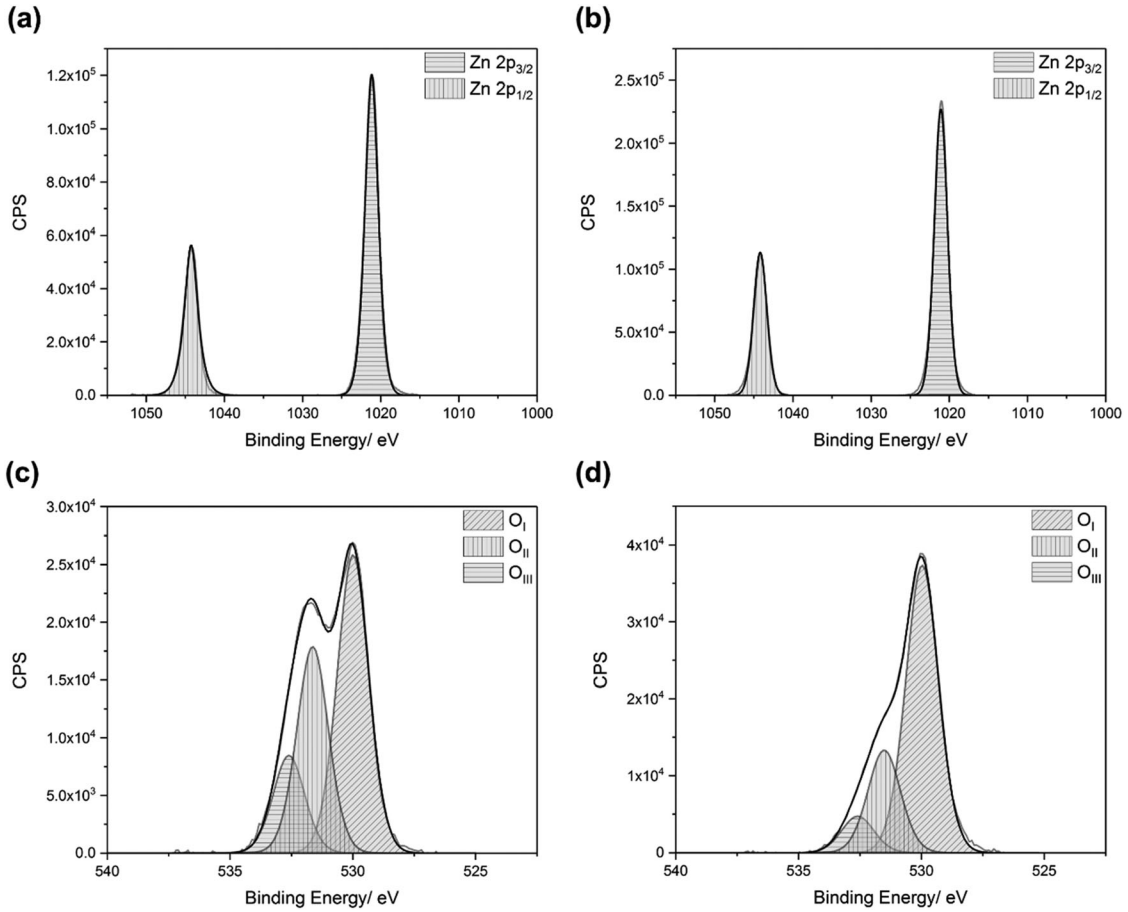

Fig. 2 Typical zinc and oxygen XPS spectra for co-doped ZnO, showing the (a) zinc 2p peaks at the surface, (b) zinc 2p peaks in the bulk, (c) oxygen 2p environments at the surface, and (d) oxygen 2p environments in the bulk. Films were deposited *via* AACVD using $Zn(acac)_2$ and MCl_3 in methanol, at a deposition temperature of 450 °C.

respectively, which matches with Al^{3+} previously reported in AZO films.[80] The gallium $3d_{5/2}$ and $3d_{3/2}$ peaks had binding energies of 20.0 eV (±0.2 eV) and 20.4 eV (±0.2 eV), respectively, which is due to Ga^{3+}.[81,82] The indium $3d_{5/2}$ and $3d_{3/2}$ peaks had binding energies of 444.9 eV (±0.2 eV) and 452.5 eV (±0.2 eV), respectively, which is due to the presence of In^{3+}.[83,84] The peaks corresponding to metallic aluminium (72.6 eV),[85] metallic gallium (18.7 eV),[86] and metallic indium (444.0 eV)[87] were not observed.

The dopant:zinc ratios at the film surfaces and within the bulks of the films were also calculated (Table 1). Each dopant was slightly surface-segregated. This is due to the formation of amorphous M_2O_3 phases at the grain boundaries, caused by the dopants reaching their solubility limit in ZnO.[88,89] These oxide phases are insulating, and limit the carrier mobility. Consequently, they result in a deterioration of the electrical properties.[90,91] The only exception to this was gallium in the AGZO film, which was bulk-segregated. Another observation that can be made from the XPS data is that, for each film, there appeared to be a preferential incorporation of the lighter dopant elements.

Surface morphology

The surface morphologies of the films were highly dopant-dependant (Fig. 4). The grains of the AGZO film were randomly shaped, with their surfaces generally oriented upwards. Moreover, the grains of this film appeared to be smooth and pristine, without any morphological defects such as nano-cracks. The grains of the IGZO film were much more hexagonal in shape. They grew in a columnar fashion, with their surfaces also facing upwards. Jayaraman *et al.* observed well-defined hexagonal grains in their IGZO films deposited *via* spray pyrolysis, which had similar diameters to the IGZO grains described in this work.[54] The grain structure of the IGZO film is very similar to the GZO film deposited previously using the same conditions.[36] In both cases, the grains grew in a similar hexagonal, columnar fashion, with very similar grain sizes. This suggests that gallium has a greater influence over the growth mechanism than indium. The AIZO film had a grain structure that was similar to that of the AGZO film, with randomly shaped grains. Because the AGZO and AIZO films had similar surface morphologies, this also indicates that aluminium had a greater influence over the growth mechanism than indium. The main difference between the AGZO and AIZO morphologies is that the AIZO film had more nano-cracks, which suggests that the use of indium was detrimental towards grain growth. This is likely because indium is the only dopant with an ionic radius larger than Zn^{2+}, resulting in a relatively

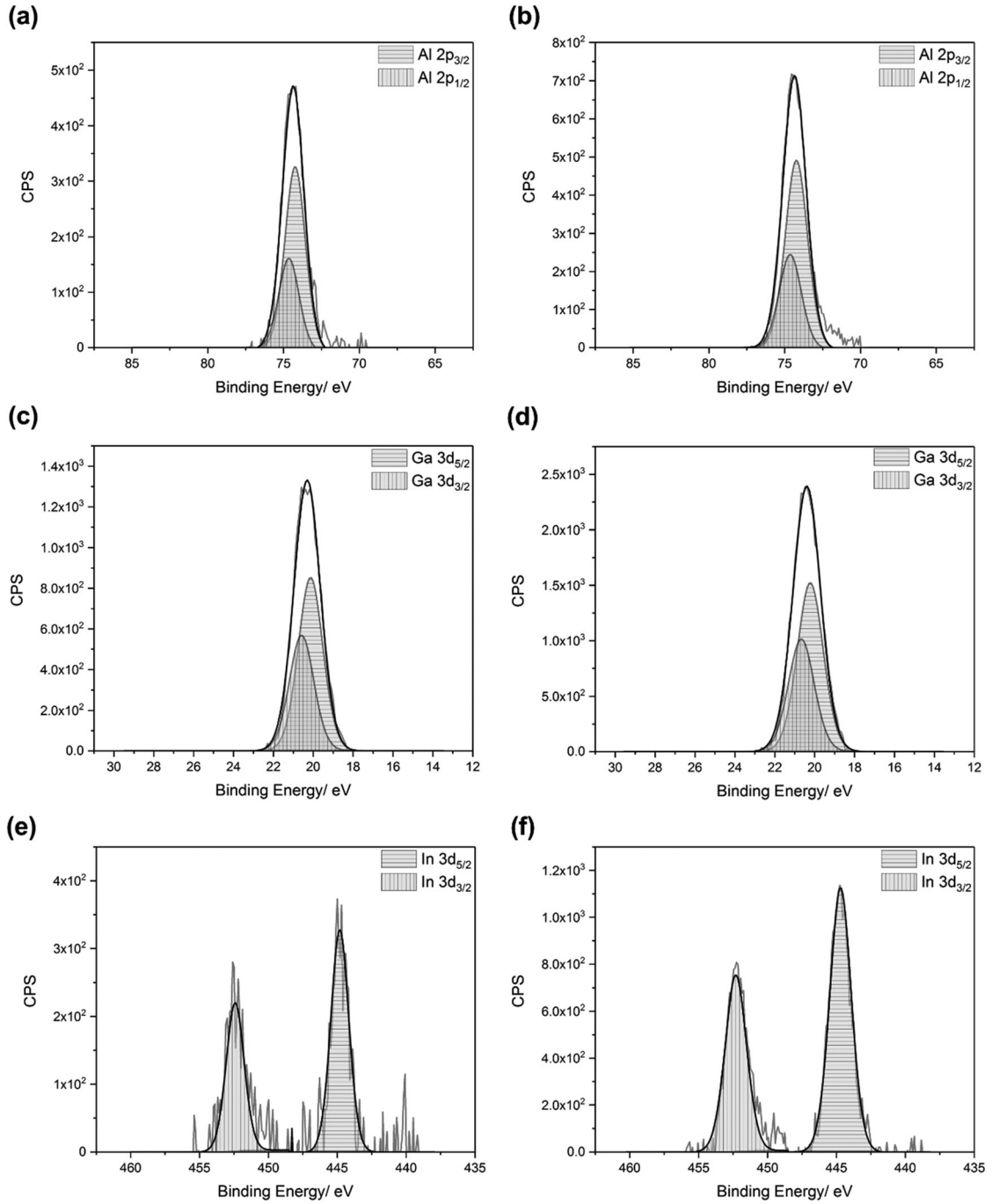

Fig. 3 Typical dopant XPS spectra for co-doped ZnO, showing the (a) aluminium 2p peaks at the surface, (b) aluminium 2p peaks in the bulk, (c) gallium 3d peaks at the surface, (d) gallium 3d peaks in the bulk, (e) indium 3d peaks at the surface, and (f) indium 3d peaks in the bulk. Films were deposited *via* AACVD using $Zn(acac)_2$ and MCl_3 in methanol, at a deposition temperature of 450 °C.

high concentration of crystal defects, leading to poorer crystal growth.

Large, well-connected grains with few defects are preferable for TCO applications to reduce grain boundary scattering.[46,92] Although grain boundary scattering is typically thought to make a smaller contribution towards carrier mobility in samples where the mean free path of the carriers is smaller than the grain size,[93] it is important to note that grain boundary scattering has a more profound effect on ZnO-based TCOs than it does on ITO.[94] This is because of the higher concentration of trap states at grain boundaries in ZnO-based TCOs compared to ITO.[95,96] Therefore, it is important to ensure that the grain structure of doped ZnO has as few morphological defects as possible.

Out of the three films deposited, the AIZO film had the most morphological defects, such as nano-cracks within the grains.

Table 1 Dopant : Zn ratios in the AGZO, IGZO, and AIZO films, as determined by XPS

	Surface concentration/atom%			Bulk concentration/atom%		
	Dopant					
Film	Al	Ga	In	Al	Ga	In
AGZO	9.6	4.2	—	9.0	4.9	—
IGZO	—	8.7	0.9	—	6.3	0.8
AIZO	4.2	—	1.8	2.1	—	1.0

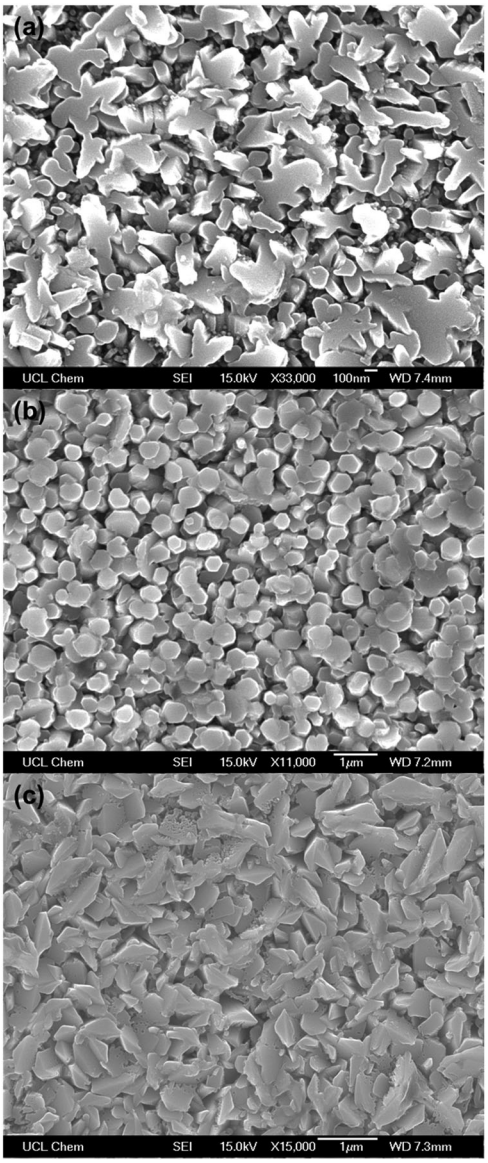

Fig. 4 SEM images of the (a) AGZO, (b) IGZO, and (c) AIZO thin films deposited *via* AACVD, using $Zn(acac)_2$ and MCl_3 in methanol, at a deposition temperature of 450 °C.

This suggests that the presence of Ga^{3+} resulted in superior grain growth. This is likely due to Ga^{3+} possessing a similar ionic radius to Zn^{2+}, thus allowing for good quality crystal growth, with relatively few defects in the structure.

Optical properties

For most TCO applications, >80% transmittance in the visible part of the spectrum (400–700 nm) is required.[97] The film with the highest visible transmittance was the AGZO film (Fig. 5). The IGZO and AIZO films had very similar transmission profiles. This suggests that the incorporation of indium resulted in an increase in optical absorption, due to the disorder introduced into the structure caused by the large radius of In^{3+}. The disorder results in the formation of localised states near the conduction band minimum. This leads to an increase in the band tail width, known as the Urbach energy.[98,99] The additional states that arise due to the structural disorder result in an increase in absorption. Generally, the more disorder that is present in the structure, the greater the Urbach tail width. The use of any dopant will cause some disorder in the structure; however, as indium is the only dopant from this work with an ionic radius larger than that of Zn^{2+}, it will result in the greatest amount of disorder. This explains the reduction in visible transmittance for the films which contain indium.

The transmission–reflectance data was used to generate Tauc plots (Fig. 6). These plots confirm the disorder introduced into the structure due the presence of indium. The Urbach energy typically manifests itself as a long wavelength absorption tail added to the main absorption edge.[100] The Urbach tails for the IGZO and AIZO films are higher in terms of absorbance than the AGZO film. The Tauc plots also revealed that the optical band gaps (E_g) of the films were not dopant-dependant, and remained constant at ~3.27–3.28 eV. In previous work, undoped ZnO deposited in the same conditions yielded a band gap of 3.16 eV.[62] Hence, the co-doped films have resulted in a widening of the band gap. This is due to the Burstein–Moss effect, whereby lower energy levels in the conduction band are filled by electrons provided by the dopant elements.[101,102] This raises the Fermi level. Hence, because the lower levels are blocked, more energy is required to promote electrons from the valence band to the conduction band.[9,29] For this reason, the optical band gap increases.[103]

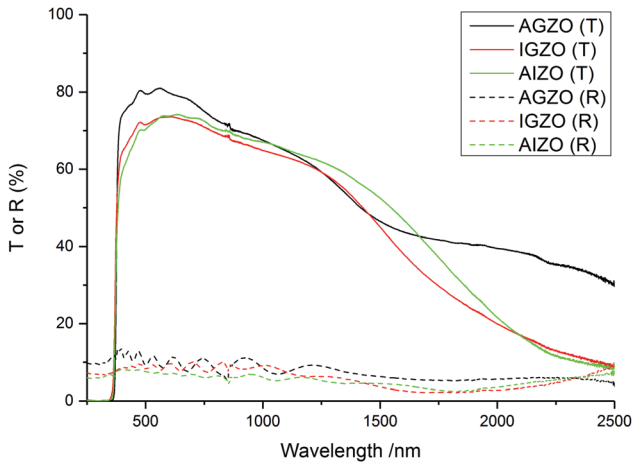

Fig. 5 Transmission–reflectance spectra of the AGZO, IGZO, and AIZO films deposited *via* AACVD, using $Zn(acac)_2$ and MCl_3 in methanol, at a deposition temperature of 450 °C.

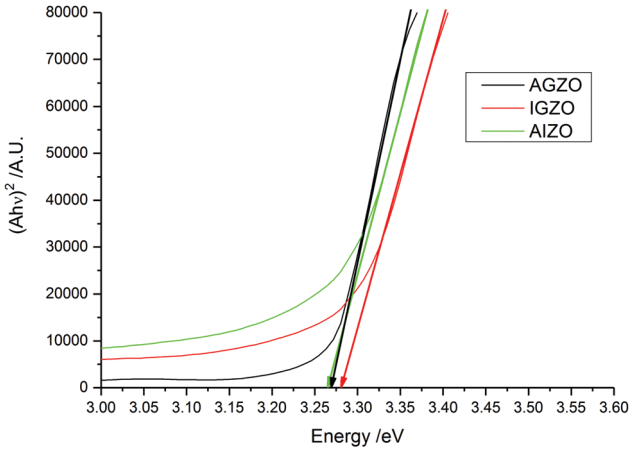

Fig. 6 Tauc plots of the co-doped AGZO, IGZO, and AIZO films deposited *via* AACVD, using $Zn(acac)_2$ and MCl_3 in methanol, at a deposition temperature of 450 °C.

Electrical properties

The electrical properties of the films were determined using the van der Pauw technique, and are summarised in Table 2. All of the films were shown to have n-type conductivity, with electrons as the majority charge carrier. The AGZO film displayed the lowest resistivity (1.3×10^{-2} Ω cm) and highest carrier mobility (7.9 $cm^2\ V^{-1}\ s^{-1}$). This may indicate that the presence of indium resulted in increased lattice distortion, resulting in poorer transport properties. The AIZO film was close to the AGZO film in terms of mobility, which suggests that the presence of aluminium partially compensated for the lattice distortion caused by indium. This could be due to Al^{3+} having a smaller ionic radius than Zn^{2+}, whereas In^{3+} has a larger radius. The IGZO film had the highest resistivity and the lowest mobility, possibly due to the fact that these dopants were the largest in terms of their radii, and hence more lattice distortion would be expected. Additionally, this film possessed smaller grain sizes, which, as previously discussed, could lead to increased grain boundary scattering, particularly for ZnO-based TCOs.

The resistivity values of these films are higher than the most conductive individually doped film (10 mol% AZO) which was deposited previously in the same conditions.[36] This could be because the total amount of dopant incorporated into the co-doped films (as indicated by XPS) was less than the total amount of dopant incorporated for the most conductive individually doped AZO film. As a result, a lower carrier concentration had been supplied to the conduction band, leading to higher resistivity.

Table 2 Typical electrical properties of the AGZO, IGZO, and AIZO films deposited *via* AACVD

Film	Resistivity × 10^{-2}/Ω cm	Carrier concentration × $10^{20}/cm^{-3}$	Carrier mobility/ $cm^2\ V^{-1}\ s^{-1}$
AGZO	1.3	1.0	7.9
IGZO	2.1	0.7	3.3
AIZO	1.6	0.8	6.8

Nguyen *et al.* reported that the resistivity of their GZO film (4.4×10^{-4} Ω cm) was lower than the resistivity of their IGZO film (9.0×10^{-4} Ω cm), both deposited *via* magnetron sputtering.[55] They explained that this was due to the lower crystallinity of the IGZO film, which led to an increase in localized states in the band structure, which subsequently acted as electron traps. Additionally, the different electronegativity values of gallium (1.81) and indium (1.78) indicate that electrons will experience a randomly fluctuating potential, which can lead to a lower carrier mobility.

The optoelectronic properties of the materials in this work are comparable or superior to several previous attempts at co-doped ZnO. Ebrahimifard *et al.* synthesised AGZO thin films on glass substrates *via* dip coating, and varied the concentrations of aluminium and gallium.[104] Their minimum resistivity value was on the order of 10^0 Ω cm. Park *et al.* deposited AGZO nanofibers films *via* electrospinning, and obtained a minimum resistivity on the order of 10^2 Ω cm.[105] Jayaraman *et al.* deposited IGZO thin films on glass substrates *via* spray pyrolysis – a technique which is closely related to AACVD. They achieved a minimum resistivity of 1.1×10^{-2} Ω cm, which is similar to the films from this work.

While co-doped ZnO films with lower resistivity values (*ca.* 10^{-4} Ω cm) have been prepared previously *via* PLD[106] and magnetron sputtering,[107] the ease of deposition using AACVD make the films from this work especially promising, and with the optimisation of deposition conditions, further improvements in the optoelectronic properties are achievable.

Conclusions

AGZO, IGZO, and AIZO thin films were deposited *via* AACVD for the first time. All of the films were pure wurtzite ZnO, with no secondary phases observed. The preferred orientation of the films was also shown to be dopant-dependant. The incorporation of aluminium promoted growth in the (002) direction, whereas indium promoted growth in the (101) direction. XPS analysis confirmed the presence of the oxidised dopants in each film. The morphologies of the films were dopant-dependant, and the presence of gallium appeared to result in superior grain growth. This is likely because the ionic radius of gallium is closer to Zn^{2+} than the other dopants, leading to higher quality crystal growth. Using indium was detrimental towards grain growth due to its large ionic radius, which caused increased crystal disorder. This disorder was observable in the transmission–reflectance spectra of the IGZO and AIZO films, and caused a higher absorbance in the visible part of the spectrum. This was confirmed by the more significant Urbach tails in the Tauc plots for the IGZO and AIZO films. The AGZO film was the most conductive, due to the high-quality crystallinity and morphology, which led to superior transport properties.

Conflicts of interest

There are no conflicts to declare.

Acknowledgements

The authors would like to thank the EPSRC for grant EP/L017709 and UCL for an impact studentship (D. B. P.), as well as NSG (Pilkington Technology Management Limited, European Technical Centre, Hall Lane, Lathom, Nr. Ormskirk, L40 5UF, UK) for their support.

References

1 S. C. Dixon, D. O. Scanlon, C. J. Carmalt and I. P. Parkin, *J. Mater. Chem. C*, 2016, **419**, 6946–6961.
2 J. L. Zhao, X. W. Sun, H. Ryu and Y. B. Moon, *Opt. Mater.*, 2011, **33**, 768–772.
3 J. Clatot, G. Campet, A. Zeinert, C. Labrugère, M. Nistor and A. Rougier, *Sol. Energy Mater. Sol. Cells*, 2011, **95**, 2357–2362.
4 U.S. Geological Survey, *Miner. Commod. Summ.*, 2017, p. 202.
5 A. Janotti and C. G. Van de Walle, *Rep. Prog. Phys.*, 2009, **72**, 126501.
6 S. J. Pearton, D. P. Norton, K. Ip, Y. W. Heo and T. Steiner, *Superlattices Microstruct.*, 2003, **34**, 3–32.
7 Ü. Özgür, Y. I. Alivov, C. Liu, A. Teke, M. A. Reshchikov, S. Doğan, V. Avrutin, S. J. Cho and H. Morko, *J. Appl. Phys.*, 2005, **98**, 1–103.
8 M. R. Waugh, G. Hyett and I. P. Parkin, *Chem. Vap. Deposition*, 2008, **14**, 366–372.
9 A. Jain, P. Sagar and R. M. Mehra, *Solid-State Electron.*, 2006, **50**, 1420–1424.
10 N. Kamarulzaman, M. F. Kasim and R. Rusdi, *Nanoscale Res. Lett.*, 2015, **10**, 346.
11 C. H. Lee and D. W. Kim, *J. Electroceram.*, 2014, **33**, 12–16.
12 R. Nasser, W. Ben, H. Othmen, H. Elhouichet and M. Férid, *Appl. Surf. Sci.*, 2017, **393**, 486–495.
13 N. Rashidi, V. L. Kuznetsov, J. R. Dilworth, M. Pepper, P. J. Dobson and P. P. Edwards, *J. Mater. Chem. C*, 2013, **1**, 6960.
14 E. Fortunato, V. Assunção, A. Gonçalves, A. Marques, H. Águas, L. Pereira, I. Ferreira, P. Vilarinho and R. Martins, *Thin Solid Films*, 2004, **451–452**, 443–447.
15 Y. H. Kim, J. Jeong, K. S. Lee, J. K. Park, Y. J. Baik, T. Y. Seong and W. M. Kim, *Appl. Surf. Sci.*, 2010, **256**, 5102–5107.
16 C.-F. Yu, S.-H. Chen, S.-J. Sun and H. Chou, *Appl. Surf. Sci.*, 2011, **257**, 6498–6502.
17 Z. C. Jin, I. Hamberg and C. G. Granqvist, *J. Appl. Phys.*, 1988, **64**, 5117–5131.
18 M. Kon, P. K. Song, Y. Shigesato, P. Frach, A. Mizukami and K. Suzuki, *Jpn. J. Appl. Phys.*, 2002, **41**, 814–819.
19 D. L. Zhu, Q. Wang, S. Han, P. J. Cao, W. J. Liu, F. Jia, Y. X. Zeng, X. C. Ma and Y. M. Lu, *Appl. Surf. Sci.*, 2014, **298**, 208–213.
20 K. Djessas, I. Bouchama, J. L. Gauffier and Z. B. Ayadi, *Thin Solid Films*, 2014, **555**, 28–32.
21 P. Gondoni, M. Ghidelli, F. Di Fonzo, V. Russo, P. Bruno, J. Martí-Rujas, C. E. Bottani, A. Li Bassi and C. S. Casari, *Thin Solid Films*, 2012, **520**, 4707–4711.
22 S.-M. Park, T. Ikegami and K. Ebihara, *Thin Solid Films*, 2006, **513**, 90–94.
23 G. Socol, D. Craciun, I. N. Mihailescu, N. Stefan, C. Besleaga, L. Ion, S. Antohe, K. W. Kim, D. Norton, S. J. Pearton, A. C. Galca and V. Craciun, *Thin Solid Films*, 2011, **520**, 1274–1277.
24 T. Ohgaki, Y. Kawamura, T. Kuroda, N. Ohashi, Y. Adachi, T. Tsurumi, F. Minami and H. Haneda, *Key Eng. Mater.*, 2003, **248**, 91–94.
25 C.-Y. Chen, L.-H. Hsiao and J.-I. Chyi, *J. Cryst. Growth*, 2015, **425**, 216–220.
26 H. Saarenpää, T. Niemi, A. Tukiainen, H. Lemmetyinen and N. Tkachenko, *Sol. Energy Mater. Sol. Cells*, 2010, **94**, 1379–1383.
27 W. J. Maeng and J.-S. Park, *J. Electroceram.*, 2013, **31**, 338–344.
28 P. R. Chalker, P. A. Marshall, S. Romani, J. W. Roberts, S. J. C. Irvine, D. A. Lamb, A. J. Clayton and P. A. Williams, *J. Vac. Sci. Technol., A*, 2013, **31**, 01A120.
29 H. Hung-Chun Lai, T. Basheer, V. L. Kuznetsov, R. G. Egdell, R. M. J. Jacobs, M. Pepper and P. P. Edwards, *J. Appl. Phys.*, 2012, **112**, 83708.
30 S. Edinger, N. Bansal, M. Bauch, R. A. Wibowo, G. Ujvari, R. Hamid, G. Trimmel and T. Dimopoulos, *J. Mater. Sci.*, 2017, **52**, 8591–8602.
31 J. Hu and R. G. Gordon, *J. Appl. Phys.*, 1992, **71**, 880–890.
32 T. Terasako, Y. Ogura, K. Ohmae, S. Fujimoto, M. Yagi and S. Shirakata, *Surf. Coat. Technol.*, 2013, **230**, 245–253.
33 J. Nishino, T. Kawarada, S. Ohshio, H. Saitoh, K. Maruyama and K. Kamata, *J. Mater. Sci. Lett.*, 1997, **16**, 2887–2890.
34 D. S. Bhachu, G. Sankar and I. P. Parkin, *Chem. Mater.*, 2012, **24**, 4704–4710.
35 J. A. Manzi, C. E. Knapp, I. P. Parkin and C. J. Carmalt, *Thin Solid Films*, 2016, **616**, 477–481.
36 D. B. Potter, D. S. Bhachu, M. J. Powell, J. A. Darr, I. P. Parkin and C. J. Carmalt, *Phys. Status Solidi*, 2016, **7**, 1346–1352.
37 A. A. Yaroshevsky, *Geochem. Int.*, 2006, **44**, 48–55.
38 A. Nebatti, C. Pflitsch, B. Curdts and B. Atakan, *Mater. Sci. Semicond. Process.*, 2015, **39**, 467–475.
39 A. Abrutis, L. Silimavicius, V. Kubilius, T. Murauskas, Z. Saltyte and V. Plausinaitiene, *Thin Solid Films*, 2015, **576**, 88–97.
40 S. Kuprenaite, T. Murauskas, A. Abrutis, V. Kubilius, Z. Saltyte and V. Plausinaitiene, *Surf. Coat. Technol.*, 2014, **271**, 156–164.
41 P. K. Jain and M. Salim, *Mater. Res. Express*, 2017, **4**, 75902.
42 B. Onwona-Agyeman, M. Nakao, T. Kohno, D. Liyanage, K. Murakami and T. Kitaoka, *Chem. Eng. J.*, 2013, **219**, 273–277.
43 J. H. Lim, S. M. Lee, H.-S. Kim, H. Y. Kim, J. Park, S.-B. Jung, G. C. Park, J. Kim and J. Joo, *Sci. Rep.*, 2017, **7**, 41992.
44 H. Wang, S. Baek, J. Song, J. Lee and S. Lim, *Nanotechnology*, 2008, **19**, 75607.
45 H. J. Ko, Y. F. Chen, S. K. Hong, H. Wenisch, T. Yao and D. C. Look, *Appl. Phys. Lett.*, 2000, **77**, 3761.
46 J. Nomoto, M. Konagai, T. Miyata and T. Minami, *J. Vac. Sci. Technol., A*, 2010, **28**, 861.

47 R. D. Shannon and C. T. Prewitt, *Acta Crystallogr., Sect. B: Struct. Crystallogr. Cryst. Chem.*, 1970, **26**, 1046–1048.
48 V. Assunção, E. Fortunato, A. Marques, H. Águas, I. Ferreira, M. E. V. Costa and R. Martins, *Thin Solid Films*, 2003, **427**, 401–405.
49 K.-W. Seo, H.-S. Shin, J.-H. Lee, K.-B. Chung and H.-K. Kim, *Vacuum*, 2014, **101**, 250–256.
50 O. Makuku, F. Mbaiwa and T. S. Sathiaraj, *Ceram. Int.*, 2016, **42**, 14581–14586.
51 V. K. Jayaraman, A. M. Álvarez, Y. M. Kuwabara, Y. Koudriavstev and M. D. L. L. O. Amador, *Mater. Sci. Semicond. Process.*, 2016, **47**, 32–36.
52 C. M. Hsu, W. C. Tzou, C. F. Yang and Y. J. Liou, *Materials*, 2015, **8**, 2769–2781.
53 H. Q. Le and S. J. Chua, *J. Phys. D: Appl. Phys.*, 2011, **44**, 125104.
54 V. K. Jayaraman, A. M. Alvarez and M. d. l. l. O. Amador, *Phys. E*, 2017, **86**, 164–167.
55 N. H. Nguyen Tran, H. T. Nguyen, Y.-R. Liu, M. Aminzare, A. T. T. Pham, S. Cho, D. P. Wong, K.-H. Chen, T. Seetawan, N. K. Pham, H. K. T. Ta, C. V. Tran and T. B. Phan, *ACS Appl. Mater. Interfaces*, 2016, **8**, 33916–33923.
56 S. Teehan, H. Efstathiadis and P. Haldar, *J. Alloys Compd.*, 2011, **509**, 1094–1098.
57 T. Tohsophon, N. Wattanasupinyo, B. Silskulsuk and N. Sirikulrat, *Thin Solid Films*, 2011, **520**, 726–729.
58 V. K. Jayaraman, A. Maldonado-Alvarez, A. E. Jimenez-Gonzalez and M. D. L. L. Olvera-Amador, *Mater. Lett.*, 2016, **181**, 52–55.
59 X. Hou and K.-L. Choy, *Chem. Vap. Deposition*, 2006, **12**, 583–596.
60 P. Marchand, I. A. Hassan, I. P. Parkin and C. J. Carmalt, *Dalton Trans.*, 2013, **42**, 9406–9422.
61 M. J. Powell, D. B. Potter, R. L. Wilson, J. A. Darr, I. P. Parkin and C. J. Carmalt, *Mater. Des.*, 2017, **129**, 116–124.
62 D. B. Potter, M. J. Powell, J. A. Darr, I. P. Parkin and C. J. Carmalt, *RSC Adv.*, 2017, **7**, 10806–10814.
63 A. Kafizas, N. Noor, P. Carmichael, D. O. Scanlon, C. J. Carmalt and I. P. Parkin, *Adv. Funct. Mater.*, 2014, **24**, 1758–1771.
64 R. Wang, L. L. H. King and A. W. Sleight, *J. Mater. Res.*, 2011, **11**, 1659–1664.
65 N. Fujimura, T. Nishihara, S. Goto, J. Xu and T. Ito, *J. Cryst. Growth*, 1993, **130**, 269–279.
66 M. Birkholz, *Phys. Rev. B: Condens. Matter Mater. Phys.*, 2003, **68**, 1–8.
67 S. C. Dixon, S. Sathasivam, B. A. D. Williamson, D. O. Scanlon, C. J. Carmalt and I. P. Parkin, *J. Mater. Chem. C*, 2017, **5**, 7585–7597.
68 M. A. Ehsan, H. N. Ming, M. Misran, Z. Arifin, E. R. T. Tiekink, A. P. Safwan, M. Ebadi, W. J. Basirun and M. Mazhar, *Chem. Vap. Deposition*, 2012, **18**, 191–200.
69 M. Ohyama, H. Kozuka and T. Yoko, *J. Am. Ceram. Soc.*, 2005, **81**, 1622–1632.
70 S. Basharat, C. J. Carmalt, R. Binions, R. Palgrave and I. P. Parkin, *Dalton Trans.*, 2008, 591–595.
71 S. Basharat, C. J. Carmalt, S. A. Barnett, D. A. Tocher and H. O. Davies, *Inorg. Chem.*, 2007, **46**, 9473–9480.
72 S. Karamat, R. S. Rawat, P. Lee, T. L. Tan and R. V. Ramanujan, *Prog. Nat. Sci.: Mater. Int.*, 2014, **24**, 142–149.
73 A. Gulino, I. Fragala, S. Chimiche and V. A. Doria, *Chem. Mater.*, 2002, **14**, 116–121.
74 H. Jung, D. Kim and H. Kim, *Appl. Surf. Sci.*, 2014, **297**, 125–129.
75 S. Chirakkara and S. B. Krupanidhi, *Phys. Status Solidi RRL*, 2012, **6**, 34–36.
76 D. J. Goyal, C. Agashe, M. G. Takwale, V. G. Bhide, S. Mahamuni and S. K. Kulkarni, *J. Mater. Res.*, 1993, **8**, 1052–1056.
77 K. Mun Wong, S. M. Alay-E-Abbas, Y. Fang, A. Shaukat and Y. Lei, *J. Appl. Phys.*, 2013, **114**, 034901.
78 B. Deng, A. Luisa da Rosa, T. Frauenheim, J. P. Xiao, X. Q. Shi, R. Q. Zhang and M. A. Van Hove, *Nanoscale*, 2014, **6**, 11882–11886.
79 J. Carrasco, N. Lopez and F. Illas, *Phys. Rev. Lett.*, 2004, **93**, 3–6.
80 D. S. Y. Jayathilake, T. A. N. Peiris, J. Sagu, D. B. Potter, K. G. U. Wijayantha, C. J. Carmalt and D. J. Southee, *ACS Sustainable Chem. Eng.*, 2017, **5**, 4820–4829.
81 R. Carli and C. L. Bianchi, *Appl. Surf. Sci.*, 1994, **74**, 99–102.
82 G. Cossu, G. M. Ingo, G. Mattogno, G. Padeletti and G. M. Proietti, *Appl. Surf. Sci.*, 1992, **56–58**, 81–88.
83 A. W. C. Lin, N. R. Armstrong and T. Kuwana, *Anal. Chem.*, 1977, **49**, 1228–1235.
84 L. L. Kazmerski, O. Jamjoum, P. J. Ireland and S. K. Deb, *J. Vac. Sci. Technol.*, 1981, **19**, 467–471.
85 R. Hauert, J. Patscheider, M. Tobler and R. Zehringer, *Surf. Sci.*, 1993, **292**, 121–129.
86 S. Evans, *Surf. Interface Anal.*, 1985, **7**, 299–302.
87 G. Hollinger, R. Skheyta-Kabbani and M. Gendry, *Phys. Rev. B: Condens. Matter Mater. Phys.*, 1994, **49**, 11159–11167.
88 M. Miki-Yoshida, F. Paraduay-Delgado, Q. Estrada-Lopez and E. Andrade, *Thin Solid Films*, 2000, **376**, 99–109.
89 S. S. Shinde, P. S. Shinde, S. M. Pawar, A. V. Moholkar, C. H. Bhosale and K. Y. Rajpure, *Solid State Sci.*, 2008, **10**, 1209–1214.
90 J.-H. Lee and B.-O. Park, *Thin Solid Films*, 2003, **426**, 94–99.
91 Y. Shigesato, S. Takaki and T. Haranoh, *J. Appl. Phys.*, 1992, **71**, 3356–3364.
92 J.-H. Kim and S.-M. Koo, *Ceram. Int.*, 2015, **41**, 37–42.
93 K. G. Saw, N. M. Aznan, F. K. Yam, S. S. Ng and S. Y. Pung, *PLoS One*, 2015, **10**, 1–17.
94 H. Liu, V. Avrutin, N. Izyumskaya, Ü. Özgr and H. Morkoç, *Superlattices Microstruct.*, 2010, **48**, 458–484.
95 K. Ellmer and R. Mientus, *Thin Solid Films*, 2008, **516**, 5829–5835.
96 K. Ellmer and R. Mientus, *Thin Solid Films*, 2008, **516**, 4620–4627.
97 D. S. Bhachu, M. R. Waugh, K. Zeissler, W. R. Branford and I. P. Parkin, *Chem. – Eur. J.*, 2011, **17**, 11613–11621.
98 S. Schönau, F. Ruske, S. Neubert and B. Rech, *Appl. Phys. Lett.*, 2013, **103**, 192108.

99 A. S. Hassanien and A. A. Akl, *J. Alloys Compd.*, 2015, **648**, 280–290.
100 F. Mozer and F. Urbach, *Phys. Rev.*, 1956, **102**, 1519–1523.
101 E. Burstein, *Phys. Rev.*, 1954, **93**, 632–633.
102 T. S. Moss, *Proc. Phys. Soc., London, Sect. B*, 1954, **67**, 775–782.
103 S. Jin, Y. Yang, J. E. Medvedeva, J. R. Ireland, A. W. Metz, J. Ni, C. R. Kannewurf, A. J. Freeman and T. J. Marks, *J. Am. Chem. Soc.*, 2004, **126**, 13787–13793.
104 R. Ebrahimifard, M. R. Golobostanfard and H. Abdizadeh, *Appl. Surf. Sci.*, 2014, **290**, 252–259.
105 M. Park and S. M. Han, *Thin Solid Films*, 2015, **590**, 307–310.
106 S. Jin-Hyun, S. Dong-Kyun, L. HeeYoung, L. Jai-Yeoul, C. Nam-In and L. Se-Jong, *J. Korean Phys. Soc.*, 2009, **55**, 947.
107 S.-C. Chang, *Int. J. Photoenergy*, 2014, **2014**, 1–6.